Van Paepegem, W. and Degrieck, J. (2002). A New Coupled Approach of Residual Stiffness and Strength for Fatigue of Fibre-reinforced Composites. *International Journal of Fatigue*, 24(7), 747-762.

A New Coupled Approach of Residual Stiffness and Strength for Fatigue of Fibre-reinforced Composites

W. Van Paepegem* and J. Degrieck

Ghent University, Dept. of Mechanical Construction and Production,
Sint-Pietersnieuwstraat 41, 9000 Gent, Belgium

Abstract

During the last decades, fibre-reinforced composites have been established as competitive materials for naval, automotive and aerospace industry. However, the fatigue behaviour of fibre-reinforced composites is so diverse and complex that present knowledge is far from complete. Two commonly used approaches to model fatigue damage are the residual stiffness and the residual strength approach. In this paper, the change in the modulus of elasticity due to fatigue damage is studied for uni-axial bending. The proposed modelling approach is new in two ways: (i) the damage growth rate – a measure for stiffness loss – is expressed by two separate terms representing the initiation and propagation phase of damage respectively, (ii) a static failure criterion is modified to represent the decreasing reserve to ultimate static strength. In that way this coupled approach of residual stiffness and strength is capable of simulating the three stages of stiffness degradation: initial decline, gradual reduction and final failure, as well as the stress redistribution due to the loss of stiffness in the damaged zones. The model has been applied to displacement-controlled bending fatigue experiments of plain woven glass/epoxy specimens.

Keywords: fatigue; composites; damage modelling; residual strength; failure criteria.

1. Introduction

Fibre-reinforced polymers are made of reinforcing fibres embedded in a polymer matrix. This makes them heterogeneous and anisotropic. The first stage of deterioration by fatigue is observable by the formation of "damage zones", which contain a multitude of microscopic cracks and other forms of damage, such as fibre/matrix interface failure and pull-out of fibres from the matrix [1-5]. Hence damage starts very early, after only a few or a few hundred loading cycles, and a sharp initial decline of the composite's stiffness is observed. This early damage is followed by a second stage of very gradual deterioration of the material, characterized by a gradual reduction of the stiffness. More serious types of damage appear in the third stage, such as fibre fracture and instable delamination growth, leading to an accelerated decline.

In this paper, it is investigated how these three stages of stiffness degradation (initial decline – gradual reduction – final failure) can be modelled. In general, three fatigue modelling approaches for fibre-reinforced polymers can be distinguished [6]: (i) fatigue life models, which do not take into account the actual damage mechanisms but use S-N curves or Goodman-type diagrams and introduce some sort of fatigue failure criterion; (ii) phenomenological models for residual stiffness/strength; and (iii) progressive damage models

* Corresponding author (Fax: +32-(0)9-264.35.87, E-mail: Wim.VanPaepegem@rug.ac.be).

or 'mechanistic' models which use one or more damage variables related to measurable manifestations of damage (transverse matrix cracks, delamination size).
The fatigue life models and residual strength models cannot be used for the intended objective of simulating the stiffness degradation during fatigue life. Indeed, both the S-N fatigue life methodology and the residual strength approach ignore the fact that an appraisal of the actual state or a prediction of the final state (when and where failure is to be expected) of the composite structure depends on the "path" of successive damage states. Indeed, the gradual deterioration of a fibre-reinforced composite – with a loss of stiffness in the damaged zones – leads to a continuous redistribution of stress and a reduction of stress concentrations in a structural component. This was already stated by – amongst others – Allen et al. [7] and Shokrieh and Lessard [8]. Moreover, measurement of strength or life during damage development in a material is not feasible, because only one such measurement can be made for one specimen, and as yet it is very difficult to compare damage states between two specimens [2].
This follow-up of the successive damage states has been addressed by the residual stiffness models and the mechanistic models. The former describe the degradation of the stiffness properties due to fatigue damage in terms of macroscopic variables, while the latter describe the deterioration of the composite material in terms of measurable manifestations of damage (matrix crack density, delamination size).
Although the mechanistic models quantitatively account for the underlying fatigue damage mechanisms, their application to the selected plain woven glass/epoxy composite material is difficult, because the fatigue damage mechanisms are complex, both in their geometry and the details of the evolution process [9]. For example, the progressive damage model by Shokrieh and Lessard [8,10-14] makes use of Hashin-type fatigue failure criteria for seven damage modes in unidirectionally reinforced laminae: fibre tension, fibre compression, fibre-matrix shearing, matrix tension, matrix compression, normal tension and normal compression. Developing these criteria for woven fabric composites, would be a cumbersome task, and would require the finite element calculation of the individual matrix and fibre stresses. Other models, such as the damage mechanics model by Talreja [15-17] are not usable either, because they cannot simulate the last stage of final failure. The elastic potential in Talreja's model [15] is derived on the assumption of small strains and small damage.
Based on these considerations, the residual stiffness approach is chosen as the framework for the model. The phenomenological residual stiffness models use the stiffness degradation as a measure for the fatigue damage. In the one-dimensional case, the macroscopic damage variable D is defined as $D = 1 - E/E_0$, where E_0 is the undamaged longitudinal stiffness and E is the stiffness at a certain moment in fatigue life. The damage variable D is a measure for the fatigue damage on the macroscopic scale. On the microscopic scale, the composite structure changes due to the appearance of matrix cracks and other forms of damage. However, for the modelling part, the composite material is still considered as an undamaged homogeneous solid, but with degraded stiffness properties. Therefore, stiffness can be used as a potential non-destructive parameter to monitor frequently or even continuously the damage which develops in a component during service [2].
Sidoroff and Subagio [18] distinguished between damage evolution in tensile and compressive regime, where the damage law depends on the applied strain amplitude, the damage itself and three material constants. Similar expressions were derived by Vieillevigne et al. [19] and Kawai [20]. Whitworth [21] recently proposed an evolution law for the ratio of the residual stiffness to the failure stiffness, where the constants depend on the applied stress and loading frequency. Yang et al. [22] developed a fatigue evolution law for the stiffness, but distinguished between fibre-dominated and matrix-dominated fatigue behaviour [23]. Brøndsted et al. [24,25] concluded from experimental results that the stiffness degradation

rate depends on some power of the stress, but this expression was only valid in the second stage of gradual stiffness reduction.
The drawback of most existing residual stiffness models is that they are not valid in all three stages of stiffness degradation, especially if the stage of final failure is concerned. In the residual stiffness approach, fatigue failure is assumed to occur when the modulus has degraded to a critical level, which has been defined by many investigators. Hahn and Kim [26] and O'Brien and Reifsnider [27] state that fatigue failure occurs when the fatigue secant modulus degrades to the secant modulus at the moment of failure in a static test. According to Hwang and Han [28] and Whitworth [21], fatigue failure occurs when the fatigue resultant strain reaches the static ultimate strain (strain failure criterion).
In this paper, a one-dimensional residual stiffness model is proposed. It aims at simulating the three stages of stiffness degradation, including final failure. To that purpose, the damage evolution law consists of two terms, separately accounting for damage initiation and propagation. The macroscopic damage variable D, defined as $D = 1 - E/E_0$, is a macroscopic measure for the fatigue damage, since the structural changes on the microscopic scale are characterized by a macroscopic reduction of the stiffness. To simulate the stage of final failure, the strength properties of the composite material must be included. Thereto, a new stress measure, the fatigue failure index, has been defined, based on a modified use of the Tsai-Wu static failure criterion. This fatigue failure index appears particularly useful to model the stage of final failure.
The fatigue damage, causing stiffness reduction, has been restricted to all intra-layer damage (matrix cracks, fibre/matrix interface failure, fibre pull-out) that is caused by pure mechanical loading with constant frequency. Although delaminations are a dominant failure mode for fibre-reinforced composite structures, they have not been included in the model. The driving mechanisms are completely different, because out-of-plane normal and shear stresses are predominantly responsible for their initiation and growth. The material and loading conditions were chosen such that delaminations did not occur in the experimental tests.
The development of the fatigue model is described, and after that, the model is applied to displacement-controlled bending fatigue experiments of plain woven glass/epoxy composites. For an accurate calculation of the changing stress states in the composite material during degradation, the model has been implemented in the commercial finite element code SAMCEF^{TM}.

2. Stiffness degradation

It is commonly accepted that for the vast majority of fibre-reinforced composite materials, the modulus decay can be divided into three stages: initial decrease, approximately linear reduction and final failure (see Figure 1).

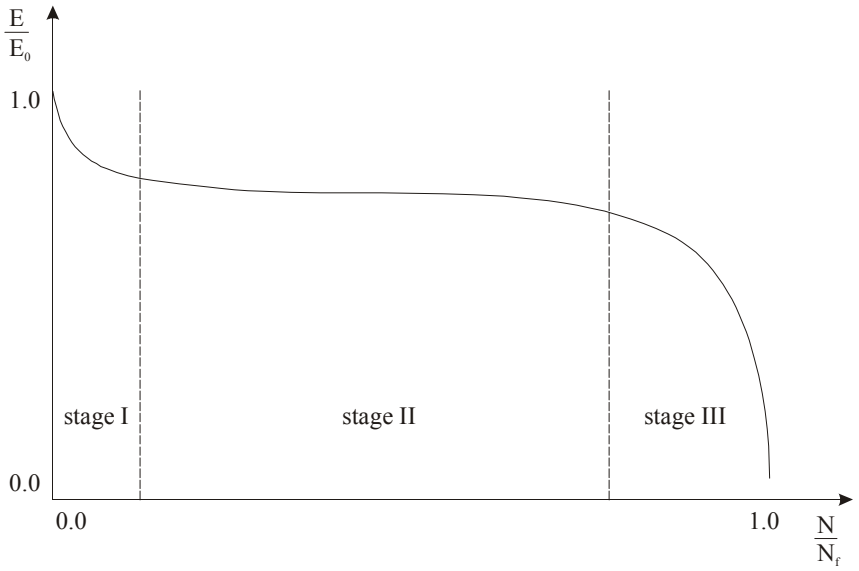

Figure 1 Typical stiffness degradation curve for a wide range of fibre-reinforced composite materials.

Early investigations on stiffness degradation were conducted by the research groups of Schulte [29-31] and Reifsnider [2,27,32].
Schulte [29-31] thoroughly studied the damage development of carbon/epoxy specimens with stacking sequence $[0,90,0,90]_{2s}$ during tension-tension fatigue (R=0.1). Schulte distinguished three distinctive stages:

- the initial region (stage I) with a rapid stiffness reduction of 2-5 %. The development of transverse matrix cracks dominates the stiffness reduction ascertained in this first stage,
- an intermediate region (stage II), in which an additional 1-5 % stiffness reduction occurs in an approximately linear fashion with respect to the number of cycles. Predominant damage mechanisms are the development of edge delaminations and additional longitudinal cracks along the 0° fibres,
- and a final region (stage III), in which stiffness reduction occurs in abrupt steps ending in specimen fracture. In stage III, a transfer to local damage progression occurs, when the first initial fibre fractures lead to strand failures.

In general, less information is available regarding fatigue behaviour when loading is fully compressive. This is mainly due to the susceptibility of composite laminates, being thin, to global buckling. This places a limitation on the unsupported length or requires some sort of buckling prevention fixture during testing. The role of the matrix and the fibre/matrix interface becomes more important in compressive loading than in tensile loading. In addition, local resin and interfacial damage lead to fibre instability in compressive loading [1,33].
Ultimately, the worst fatigue loading condition for composite materials is fully reversed axial fatigue, or tension-compression loading [1]. In compression, tensile-induced local layer delaminations can lead to local layer instability and layer buckling, perhaps before resin and interfacial damage within the layers has initiated fibre micro-buckling [34]. Further, Gamstedt and Sjögren [35] have demonstrated that there is an accelerated transverse crack initiation in tension-compression loading, due to the increased debond propagation in compression.

In this paper, displacement-controlled bending fatigue tests have been used to provide the experimental results. This type of experiments was preferred because they allow to test the

model and its finite element implementation in more complicated fatigue testing conditions than the uni-axial tension fatigue tests. Figure 2 shows a schematic drawing: one side of the specimen is clamped, while a sinusoidal displacement with amplitude u_{max} is imposed at the other side of the specimen.

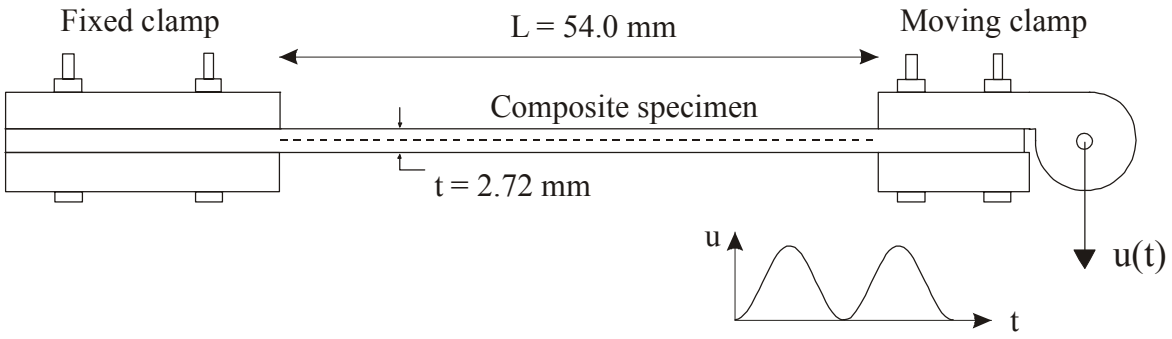

Figure 2 Schematic drawing of the bending fatigue setup.

At the clamped cross-section, the tensile stresses have their maximum value and damage is growing fast. During fatigue life, load is then gradually transferred to the underlying zones and the neutral fibre is moving towards the compressive zone. Due to the smaller bending moments, damage growth is smaller away from the fixation.

The material used in the bending fatigue experiments, was a glass fabric/epoxy composite. The fabric was a Roviglass R420 plain woven glass fabric (Syncoglas) and the epoxy was Araldite LY 556 (Ciba-Geigy). The plain woven glass fabric was stacked in eight layers, denoted as $[\#0°]_8$, where '0°' means that the warp direction of each of the eight layers has been aligned with the loading direction and where the symbol '#' refers to the fabric reinforcement type. All composite specimens were manufactured using the resin-transfer-moulding technique. After curing they had a thickness of 2.72 mm.

The force was experimentally measured by a strain gauge bridge and represents the force necessary to impose the bending displacement with constant amplitude u_{max}. Due to the (bending) stiffness degradation, this force will decrease during fatigue life. Figure 3 shows a typical example of an experimentally measured force-cycle history in single-sided bending for u_{max} = 30.4 mm. The force degradation is very similar with the stiffness degradation in tension-tension fatigue tests, as was shown in Figure 1.

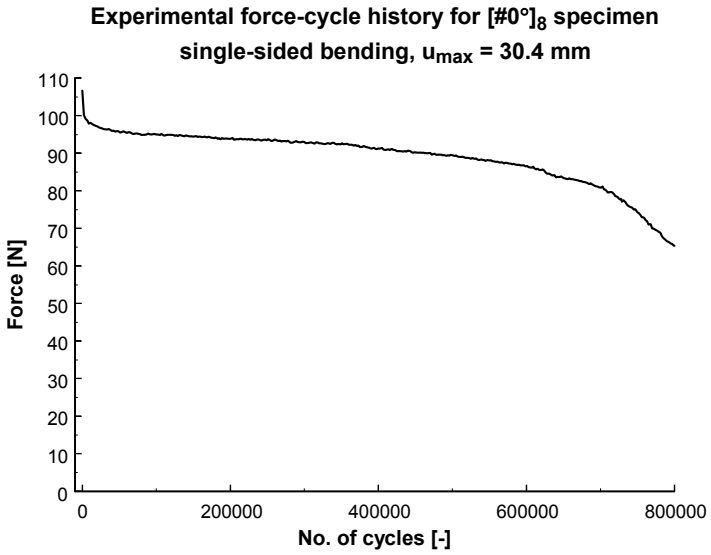

Figure 3 **Experimentally measured force-cycle history for $[\#0°]_8$ specimen.**

The developed residual stiffness model aims at simulating the full force-cycle history of the bending fatigue tests, from initial decline to final failure.

The plain woven glass/epoxy material has been homogenized into a homogeneous orthotropic material, and the elastic and strength properties of the homogenized glass/epoxy lamina have been measured experimentally. The model developed is one-dimensional in nature, and only the longitudinal stiffness (along the bending direction) is considered. As the warp direction of each layer of the $[\#0°]_8$ laminate is aligned with the loading direction, the longitudinal stiffness corresponds with the orthotropic elastic property E_{11}. The longitudinal stiffness will be further designated as the stiffness E, where E_0 is the initial modulus of the undamaged homogenized material.

The scalar damage variable D, defined as $D = 1 - E/E_0$, is a macroscopic measure for the fatigue damage, since the structural changes on the microscopic scale (matrix cracks, fibre/matrix interface failure,…) are characterized by a macroscopic reduction of the stiffness. The constitutive equations between stress, strain and damage are provided by the Continuum Damage Mechanics theory and are summarized below.

In 1958, Kachanov [36,37] proposed to describe brittle creep rupture under uni-axial tension by a scalar field variable, the continuity ψ. To a completely defect free material was ascribed the condition $\psi = 1$, whereas $\psi = 0$ was defined to characterize a completely destroyed material with no remaining load carrying capacity. The continuity ψ may be said to quantify the absence of material deterioration. The complementary quantity $D = 1 - \psi$ is therefore a measure of the state of deterioration or damage. For a completely undamaged material $D = 0$, whereas $D = 1$ corresponds to a state of complete loss of integrity of the material structure. The designation ω is also commonly used in literature.

In 1969, Rabotnov [38] introduced the concept of effective stress $\tilde{\sigma}$. The effective stress is the stress calculated over the effective area of the damaged cross-section that resists the forces:

$$\tilde{\sigma} = \frac{F}{A(1-D)} = \frac{\sigma}{1-D} \tag{1}$$

Lemaitre [39] introduced the concept of strain equivalence which states that a damaged volume of material under the nominal stress σ shows the same strain response as a comparable undamaged volume under the effective stress $\tilde{\sigma}$. Applying this principle to the elastic strain, the relation is [40]:

$$\varepsilon_e = \frac{\tilde{\sigma}}{E_0} = \frac{\sigma}{E_0(1-D)} \tag{2}$$

where E_0 is the stiffness of the undamaged material. As such, the damage variable D becomes a measure of stiffness degradation:

$$D = 1 - \frac{E}{E_0} \tag{3}$$

Research was further elaborated, amongst others, by Lemaitre [40], Chaboche [41,42], Krajcinovic [40,43] and Sidoroff [44]. These efforts evolved in the "Continuum Damage Mechanics" theory which can generally be defined as "… mechanical and phenomenological models of the material degradation leading to failure and aimed at durability predictions and including mechanical weakening" [44].

This framework is now used to establish a damage growth law of the form:

$$\frac{dD}{dN} = f_i(\sigma, D, ...) + f_p(\sigma, D, ...) \tag{4}$$

where the damage variable D is a measure for the stiffness reduction in the considered material element due to matrix cracks, fibre/matrix debonding, fibre pull-out,… The growth rate dD/dN is the damage increment per cycle N and f_i is a function which describes the first stage of damage initiation, while f_p is a function which describes the second and third stage of damage propagation and final failure, respectively.

In his survey about life prediction analysis, Reifsnider [32] also made a clear distinction between damage initiation and damage growth in the fatigue life of composite materials, although this distinction was not explicitly made in his own model. Reifsnider [45] introduced a strength degradation parameter and further distinguished between critical and sub-critical elements. The sub-critical elements control the process of internal stress redistribution and define the changes in the local stress state, while the critical elements control the failure process itself. However, the constitutive equations of his model were not separated into distinct phases of initiation and propagation.

Damage growth rate equations of phenomenological residual stiffness models have rarely if ever been expressed with a clear distinction between damage initiation and damage propagation, although research on the impact behaviour of composite materials at the authors' department has shown that damage growth rate equations which discriminate between damage initiation and damage propagation lead to very good results [46,47].

The general layout of the damage initiation and propagation functions is based on a sound combination of existing models in open literature. Although these models of previous investigators themselves are not capable of simulating the three stages of stiffness degradation, they will be integrated in a unified model that will manage to simulate the successive stages of stiffness reduction. Thereto, additional requirements for a sound modelling of the underlying fatigue damage mechanisms will be formulated and the model

will be refined to meet these demands. This two-step approach should give a clear explanation of the followed fatigue modelling strategy.

As mentioned earlier, the first stage of stiffness reduction is mainly due to the development of transverse matrix cracks, which should be modelled by the damage initiation function $f_i(\sigma,D,\ldots)$. Therefore, this function is based on existing models which correlate the extent of matrix cracks with the resulting stiffness reduction. The work of Ogin et al. [48] and Beaumont [49,50] is particularly useful in this context. They investigated matrix cracking and stiffness reduction during fatigue of a $[0°/90°]_s$ glass fibre-reinforced laminate. It was observed that the experimental measurements of stiffness degradation could be approximated over a wide range by the relation:

$$E = E_0(1 - c\delta) \tag{5}$$

where E is the modulus of the cracked composite, E_0 is the modulus of the uncracked composite, c is a constant and δ is the average crack density, defined as:

$$\delta = \frac{1}{2s} \tag{6}$$

where 2s is the average crack spacing. Ogin et al. then calculated that the growth rate of the average crack density δ could be written as:

$$\frac{d\delta}{dN} \propto \left(\frac{\sigma_{max}^2}{\delta} \right)^2 \tag{7}$$

As the crack density δ on the microscopic scale leads to a macroscopic reduction of stiffness, a similar formulation can be used for the initiation function of the macroscopic damage variable D. Hence, Equation (7) is modified into:

$$f_i(\sigma, D, \ldots) = c_1 \left(\sigma^*\right)^m e^{-c_2 D} \tag{8}$$

where D is the scalar damage variable lying between zero (virgin material) and one (final failure) as explained in Equation (3), σ^* is some measure of the stress which will be defined below, m is the power of the stress, and c_1 and c_2 are two constants. Because the factor $1/\delta$ in Equation (7) is infinite when δ equals zero (virgin material: crack spacing 2s is infinite), the factor has been replaced by the expression $\exp(-c_2 D)$.

The damage propagation function f_p is based on the work of Brøndsted et al. [24,25] who studied the fatigue damage accumulation and lifetime prediction of glass fibre-reinforced composites under block loading and stochastic loading. They observed that *stage II* of the stiffness degradation curve could be approximated by a linear relation between stiffness and number of cycles:

$$\frac{E}{E_1} = A \cdot N + B \tag{9}$$

where E is the cyclic modulus after N cycles, E_1 is the initial cyclic modulus, and A and B are constants. It was found that the constant A was a function of the maximum fatigue stress σ, normalized by the static modulus E_0. The rate of change in stiffness then becomes:

$$\frac{d\left(\frac{E}{E_1}\right)}{dN} = -K\left(\frac{\sigma}{E_0}\right)^n \tag{10}$$

where K and n are constants.
For this case, Equation (10) is modified into the equation:

$$f_p(\sigma, D, ...) = c_3\left(\sigma^*\right)^n \tag{11}$$

This damage propagation function represents the gradual decrease of stiffness in stage II.
So far, a general layout of the model has been established (Equation (8) and (11)), based on a sound combination of existing models in literature. Now, the authors' contribution will consist in defining the stress measure σ^* and next, refining the damage initiation and propagation functions into their final form.

3. Definition of the stress measure σ^*

The stress measure σ^* should represent, in each material point, the actually applied stress which can vary during fatigue life (for example, due to stress redistributions). Although the present fatigue model is based on the residual stiffness approach, there should be a correlation between the applied stress amplitude σ and the ultimate static strength of the laminate at each moment of time. This would alleviate the classical problem of residual stiffness models, namely that there is no distinct criterion for final failure. Fatigue failure is most often assumed to occur when the modulus has degraded to a critical level which is not unique and has been defined by many investigators. Already in the early 70s, Salkind [51] suggested to draw a family of S-N curves, being contours of a specified percentage of stiffness loss, to present fatigue data. Hahn and Kim [26] and O'Brien and Reifsnider [27] proposed that fatigue failure occurs when the fatigue secant modulus degrades to the secant modulus at the moment of failure in a static test. According to Hwang and Han [28], fatigue failure occurs when the fatigue resultant strain reaches the static ultimate strain.
To include the notion of strength into the fatigue damage model, the well known Tsai-Wu failure criterion is used in a modified way. Consider the one-dimensional case of the Tsai-Wu quadratic failure criterion [52,53]:

$$\frac{1}{X_T \cdot |X_C|}\sigma^2 + \left(\frac{1}{X_T} - \frac{1}{|X_C|}\right)\sigma < 1 \tag{12}$$

where X_T and X_C are the ultimate tensile and compressive static strength, respectively.
In its original form the Tsai-Wu criterion is not usable, because it only indicates whether or not the laminate fails, but gives no continuous evaluation of the margin to final failure. Moreover the sign of the criterion depends on the ratio of the tensile strength to the compressive strength.

A more attractive interpretation of the Tsai-Wu criterion was given by Liu and Tsai [54]. They calculated the so-called strength ratio R from:

$$\left(\sigma^2 \frac{1}{X_T \cdot |X_C|}\right) R^2 + \left[\sigma\left(\frac{1}{X_T} - \frac{1}{|X_C|}\right)\right] R - 1 = 0 \tag{13}$$

where the strength ratio R defines the reserve factor to failure. If R = 1, failure occurs, while if R = 2, the factor of safety is 2. An important drawback of this definition is that the strength ratio R does not change proportionally with the applied stress σ. Therefore, the failure index, defined by Liu and Tsai [54] as the inverse value of the strength ratio R, is better suited. It can be seen in Figure 4 that the failure index Σ = 1/R increases proportionally with the applied stress. Moreover, the failure index for applied tensile stresses is independent of the value of the compressive strength X_C, and vice versa.

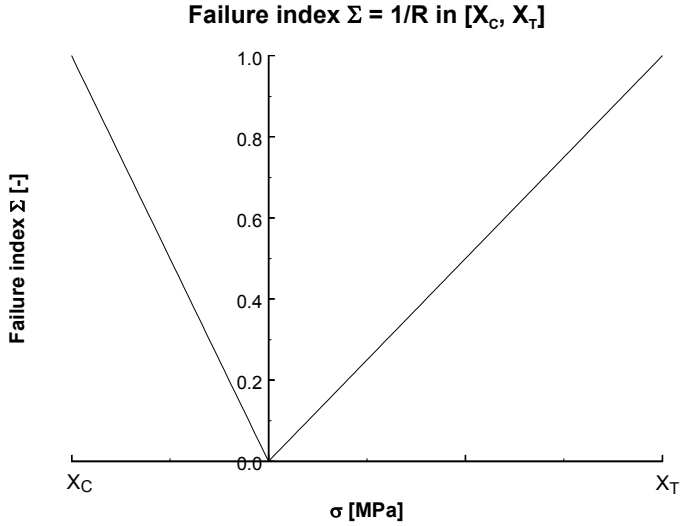

Figure 4 Graph of the failure index Σ = 1/R.

Next it is clear that the static Tsai-Wu criterion cannot be used straightforwardly as a criterion in the fatigue damage model. According to the general idea of the residual strength models [55-59], X_T and X_C should be decreasing functions of the number of cycles as well. It is rather obvious to introduce the damage variable D into the Tsai-Wu criterion instead of the number of cycles to express the influence of fatigue damage, but then the relation between the residual tensile strength σ_{RT} (= $X_T(N)$), the residual compressive strength σ_{RC} (= $X_C(N)$) and D still needs to be established.

Since the degradation curve of the strength is very similar in shape with the stiffness degradation curve for most common materials (see for example Shokrieh and Lessard [8,10-14] and Lee and Jen [60,61]), the function $\sigma_{RT} = X_T (1\text{-}D)^p$ is now postulated as a suitable expression. It is very unlikely that the power *p* would be greater than 1.0, because this would imply that the strength degradation occurs faster than the stiffness degradation. When the power p would be smaller than 1.0, the behaviour is not adequate as well, because the tensile stress is then degrading faster than the residual strength which leads to an increasing strength factor R and thus a decreasing failure index Σ. Figure 5 illustrates this with a simple numerical example which shows the evolution of stress σ, residual strength σ_{RT} and failure

index Σ with damage, for a constant strain amplitude ε = 0.003, p = 0.5, E_0 = 20 GPa and X_T = 100 MPa.

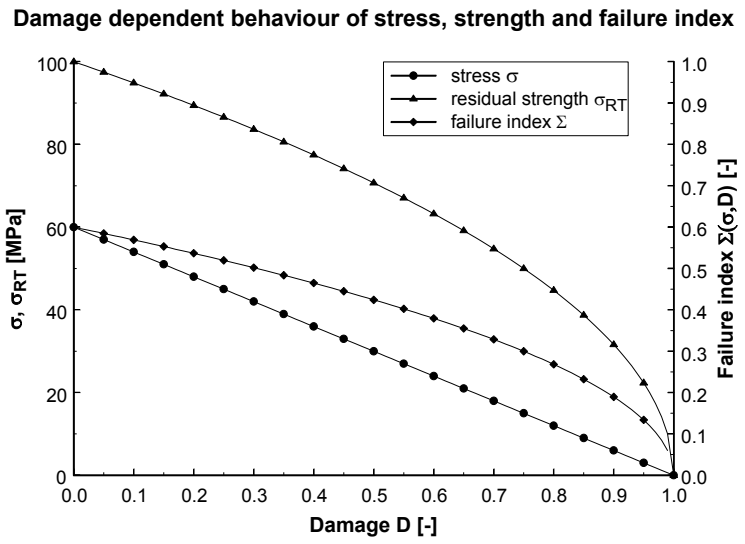

Figure 5 Evolution of stress, strength and failure index with damage (p < 1).

As the failure index Σ should remain a measure for the ratio to failure strength, even under fatigue, the failure index Σ should increase when fatigue damage D increases, but in the example, the failure index decreases to zero instead. An inspection of the cause leads to the following conclusion: since the stress degrades linearly with the damage variable D and the residual strength σ_{RT} only degrades with $\sqrt{1-D}$ (p = 0.5), the failure index Σ, defined as 1/R, is decreasing, because the strength factor R increases. For example, when E/E_0 equals 0.1 (D = 0.9), the tensile stress σ equals 6.0 MPa, while the residual strength σ_{RT} is still 31.62 MPa.
The only value for the power p which has not been considered yet, is: p = 1. The value p = 1.0 results in the following expression for the strength factor R:

$$\left[\frac{\sigma^2}{X_T(1-D)\cdot|X_C|}\right]R^2+\left[\sigma\left(\frac{1}{X_T(1-D)}-\frac{1}{|X_C|}\right)\right]R-1=0 \qquad (14)$$

The positive root of Equation (14) is $R = X_T(1-D)/\sigma$. It can be easily calculated however that the strength factor R, and hence the failure index Σ, is the same for the one-dimensional case when the residual strength σ_{RT} is kept equal to the static strength X_T and the stress σ is replaced by the effective stress $\tilde{\sigma}$ (see Equation (1)):

$$\left[\left(\frac{\sigma}{1-D}\right)^2\frac{1}{X_T\cdot|X_C|}\right]R^2+\left[\frac{\sigma}{1-D}\left(\frac{1}{X_T}-\frac{1}{|X_C|}\right)\right]R-1=0 \qquad (15)$$

When this expression is considered, a different interpretation of the concept of "residual strength" is possible: *fatigue failure occurs when the effective stress σ/(1-D) equals the initial static strength X_T, and the material static strength only decreases apparently during fatigue*

life because the measured failure load with residual strength tests is divided by the initial cross-section A_0 and not by the actual cross-section $A_0(1-D)$.
This is very similar with the tensile stress-strain curve for steel. When the strain is increased in the strain hardening domain, the cross-sectional area will decrease, but this decrease is fairly uniform over the specimen's entire gauge length. The nominal stress, defined as the load divided by the initial cross-sectional area, increases up to the ultimate stress. When the strain further increases, necking of the specimen occurs, the cross-sectional area begins to decrease in a localized region of the specimen, and the nominal stress decreases until the fracture stress is reached [62]. However when the true stress is used, defined as the load divided by the actual cross-sectional area at the instant that the load is measured, then it appears that the actual area within the necking region is always decreasing until fracture, and so the material actually sustains increasing stress !
A very analogous reasoning is followed here: fatigue loading induces damage which reduces the actual load-bearing cross-sectional area. Therefore the effective stress $\sigma/(1-D)$ is increasing and when this effective stress reaches the ultimate static strength X_T, final failure occurs. This reasoning is not at all in contradiction with the residual strength approach. During fatigue testing, the induced damage can be of a different type from the damage that is caused by static tensile tests. As a consequence, the load-bearing area is reduced (as compared to the static test) and the residual strength is smaller than the initial static strength. Evidence can be found in the work of Schulte [29-31]. He observed that "… *the damage mechanisms occurring in stage II seem to be the typical fatigue mechanics, whereas the damage mechanisms which can be observed during stage I, also occur in static tests*". Moreover, in a quasi-static tensile test, stress redistribution is not present, while this can develop during fatigue loading.
Figure 6 illustrates the difference and similarity between the two concepts for the case of a constant strain amplitude.

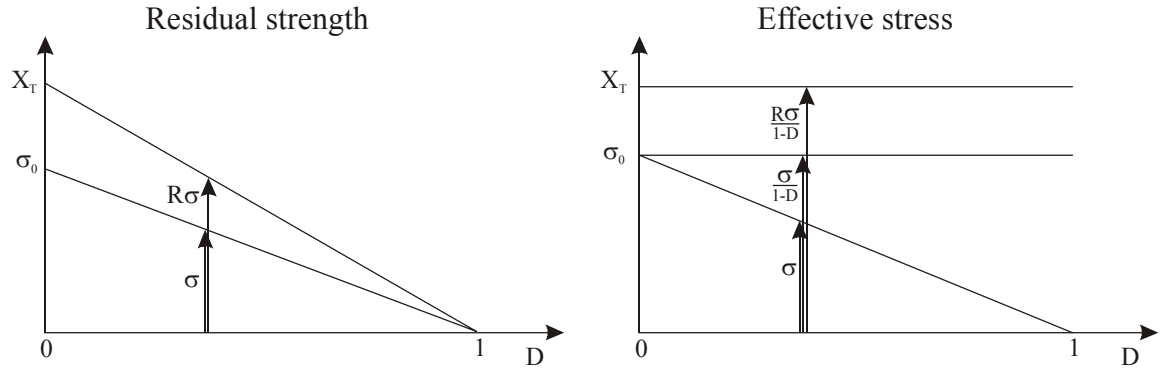

Figure 6 Illustration of the two different interpretations: residual strength and effective stress.

Summarized, the fatigue failure index $\Sigma(\sigma, D)$ is defined as 1/R, where R is the calculated safety factor to failure from the Tsai-Wu static failure criterion, where the nominal stress is replaced by the effective stress. In the one-dimensional case, it can be easily calculated that:

$$\Sigma(\sigma, D) = \frac{1}{R} = \frac{\tilde{\sigma}}{X} = \frac{\dfrac{\sigma}{1-D}}{X} = \frac{E_0 \varepsilon}{X} \qquad (X = X_T, X_C) \tag{16}$$

Indeed, as the effective stress $\sigma/(1-D)$ equals $E_0 \cdot \varepsilon$ (Equation (2)), the fatigue failure index $\Sigma(\sigma, D)$ is a measure for the applied fatigue strain. The main characteristics of the fatigue failure index $\Sigma(\sigma, D)$ are:

- it is proportional with the effective stress $\tilde{\sigma}$, or equivalently, with the applied strain ε,
- its value is dimensionless, and lying between zero ($\sigma = 0$) and one ($\sigma = X_T$ or $\sigma = X_C$),
- there is a correlation with the strength, so that final failure under fatigue loading can be predicted,
- by using a static failure criterion, the extension of the fatigue failure index definition to multi-axial loading conditions is possible,
- the definition of the fatigue failure index does not require any new relations to be established between the residual tensile/compressive strength and the fatigue damage.

The fatigue failure index $\Sigma(\sigma, D)$ can therefore be accepted as a suitable stress measure σ^*.

4. Development of the final fatigue damage model

Now that the fatigue failure index $\Sigma(\sigma, D)$ has been defined as a suitable representation for the stress measure σ^*, the last step comprises the final refinement of the expressions for damage initiation and propagation. The preliminary layout of the damage initiation and propagation functions was (see Equations (8) and (11)):

$$\frac{dD}{dN} = c_1 \left[\Sigma(\sigma, D)\right]^m e^{-c_2 D} + c_3 \left[\Sigma(\sigma, D)\right]^n \tag{17}$$

Through the definition of the fatigue failure index $\Sigma(\sigma, D)$, the damage growth rate equation dD/dN becomes strain-driven for a given material and thus for given material properties. This is very important, because when simulating load-controlled fatigue tests (nominal stress σ is constant), strain and effective stress are increasing and as a consequence the failure index Σ, calculated from Equation (15), will increase up to its failure value of one.
The model will now be modified into its final form. Based on theoretical considerations and a sound modelling of the observed fatigue damage mechanisms, the damage initiation and damage propagation function will be refined.

4.1 Damage initiation function

First the damage initiation function is addressed. This function should simulate the sharp decline of the stiffness in the first stage of fatigue life. The following observations can be made:

- it is well known that matrix cracking is the predominant mechanism in this stage and that after a sufficient number of loading cycles, the number of cracks saturates into a "Characteristic Damage State" [2-3,31]. It has been shown by Boniface et al. [63] that this saturation of matrix cracks is reached as well for woven glass fabric reinforcements,
- Schulte et al. [29] have shown that even if the maximum cyclic strain in each consecutive load cycle is below the threshold for transverse cracking under monotonic tension, cracks do develop after a number of loading cycles,

- as the failure index $\Sigma(\sigma, D)$ is constant for strain-controlled fatigue experiments, the saturated crack density should depend on the level of the cyclic strain amplitude applied.

Bearing in mind these considerations, the damage initiation function is transformed into:

$$f_i(\sigma, D) = c_1 \cdot \Sigma(\sigma, D) \cdot \exp\left(- c_2 \frac{D}{\sqrt{\Sigma(\sigma, D)}} \right) \tag{18}$$

where c_1 and c_2 are material constants. The constant c_1 determines the amplitude of the damage initiation rate, while the exponential function is a decreasing function of damage D; so once a certain damage value has been reached, the contribution of the damage initiation function becomes negligible. However, the saturating damage level depends on the amplitude of the applied strain through the factor $\sqrt{\Sigma(\sigma, D)}$.

The damage initiation function in Equation (18) does not distinguish between damage growth for tensile and compressive stresses. Moreover, in general, damage would be predicted to increase much faster under compressive loading. Indeed, the compressive strength X_C is most often smaller than the tensile strength X_T, so the fatigue failure index would be larger for the compressive stress than for the tensile stress.

This behaviour of the damage initiation function does not correspond with the experimental observations in the bending fatigue tests. Indeed, in single-sided bending, one side of the specimen is subjected to tensile stresses, while the other side is subjected to compressive stresses, and these stresses do not change sign during one fatigue loading cycle, although it is possible that due to the stress redistribution, material points are loaded with compressive stresses at the beginning of fatigue life, but end up in the tensile zone when fatigue loading continues [64,65]. In these experiments, it was observed that for small to moderate bending moments, no damage could be observed at the compression side of the specimen. Only for very large bending moments, the matrix was shattered at the surface subjected to compressive stresses. This confirms with the general meaning that damage growth rate in compression is smaller, when two restrictions are made: (i) there are no delaminations, (ii) the stress ratio R is not negative. Indeed, it is well known that the stress ratio R = -1 is very detrimental for stacking sequences which can develop delaminations. However, with the material under study, delaminations are not present due to the choice of the stacking sequence, and in single-sided bending, the stress ratio R is zero for each material point.

Thus a distinct approach for damage in compression/tension regime is necessary. In the authors' opinion, it seems appropriate to incorporate the different damage development in tension/compression regime into the damage initiation function itself. When implementing the damage law into numerical applications, it is easier to make a distinction on the level of the damage growth rate equation dD/dN, because the damage increment is calculated after each cycle and this damage increment is extrapolated to the next simulated cycle. Taking into account the above mentioned considerations, the damage initiation function finally becomes:

$$f_i(\sigma, D) = \begin{cases} c_1 \cdot \Sigma(\sigma, D) \cdot \exp\left(- c_2 \dfrac{D}{\sqrt{\Sigma(\sigma, D)}} \right) & \text{if } \sigma \geq 0 \\ \left[c_1 \cdot \Sigma(\sigma, D) \cdot \exp\left(- c_2 \dfrac{D}{\sqrt{\Sigma(\sigma, D)}} \right) \right]^3 & \text{if } \sigma < 0 \end{cases} \tag{19}$$

It is true that the presence of the third power in the damage initiation function for compressive stresses (Equation (19)) cannot be rigorously derived from theoretical considerations, but a similar distinction between tensile and compressive stresses has been applied by, amongst others, Sidoroff and Subagio [18] who used the same definition for the damage variable D (= $1 - E/E_0$) and defined the damage increment per cycle as:

$$\frac{dD}{dN} = \begin{cases} \dfrac{A(\Delta\varepsilon)^c}{(1-D)^b} & \text{in tension} \\ 0 & \text{in compression} \end{cases} \tag{20}$$

where $\Delta\varepsilon$ is the strain amplitude and A, b and c are three constants. However, Sidoroff and Subagio [18] did not distinguish between damage initation and propagation, and their model could not predict final failure.
Further it has appeared from a large set of numerical simulations that the equation (19) in its present form is very well capable of predicting the damage initiation regime (see discussion below).

4.2 Damage propagation function

The damage propagation term, as defined in Equation (17), is not zero when D = 0. This is not logical, since the first term should properly describe damage initiation on its own. To that purpose, the propagation function is multiplied with the value of D itself, so that for small values of the damage variable D, the contribution of the damage propagation function is negligible.
Secondly, the third stage of stiffness degradation is characterized by fibre fracture which leads to final failure of the composite component. This stage is not properly modelled, since there is no significant change in the growth rate dD/dN when the fatigue failure index $\Sigma(\sigma, D)$ approaches its failure value 1.0. Therefore a damage acceleration factor is added to the damage propagation function:

$$f_p(\sigma, D) = \begin{cases} c_3 \cdot D \cdot \Sigma(\sigma,D)^2 \cdot \left[1 + \exp\left(c_5\left(\Sigma(\sigma,D) - c_4\right)\right)\right] & \text{if} \quad \sigma \geq 0 \\ c_3 \cdot D \cdot \Sigma(\sigma,D)^2 \cdot \left[1 + \exp\left(\dfrac{c_5}{3}\left(\Sigma(\sigma,D) - c_4\right)\right)\right] & \text{if} \quad \sigma < 0 \end{cases} \tag{21}$$

Each of the constants has a well-defined meaning: c_3 is the damage propagation rate, c_4 is a sort of threshold below which no fibre fracture initiates. Once the threshold has been crossed and initial fibre fracture occurs, the exponential function fastly increases and forces final failure of that particular material point. Of course, the constant c_5 must have a large value, so that the power of the exponential function remains strongly negative as long as the failure index $\Sigma(\sigma, D)$ remains below the threshold c_4, but switches to a large positive value once the threshold has been crossed. Similar to the initiation function, a factor 3 has been introduced in the damage acceleration factor for compressive regime, because it was again observed that failure occurs in a less brutal manner than at the tensile side.

4.3 Final layout of the fatigue damage model

The definitive form of the damage initiation and propagation functions then becomes:

$$\frac{dD}{dN} = \begin{cases} c_1 \cdot \Sigma \cdot \exp\left(-c_2 \frac{D}{\sqrt{\Sigma}}\right) + c_3 \cdot D \cdot \Sigma^2 \cdot \left[1 + \exp\left(c_5 (\Sigma - c_4)\right)\right] & \text{if } \sigma \geq 0 \\ \left[c_1 \cdot \Sigma \cdot \exp\left(-c_2 \frac{D}{\sqrt{\Sigma}}\right)\right]^3 + c_3 \cdot D \cdot \Sigma^2 \cdot \left[1 + \exp\left(\frac{c_5}{3}(\Sigma - c_4)\right)\right] & \text{if } \sigma < 0 \end{cases} \tag{22}$$

When the stress is zero, the failure index $\Sigma(\sigma, D)$ is zero and the damage growth rate is zero.
Although the model is based on the residual stiffness approach, it can provide predictions about the residual strength as well. Indeed, if for example the model predicts a damage value $D = 0.3$ when the specimen has been subjected to a uni-axial tensile fatigue test, then the specimen should fail in a subsequent static tensile test when:

$$\tilde{\sigma} = \frac{\sigma}{1 - D} = \frac{\sigma}{1 - 0.3} = X_T \tag{23}$$

This is equivalent with the statement in the classical residual strength approach, that the static strength has decreased with 30 % due to the applied tensile fatigue testing.
In the next paragraph, the finalized fatigue damage model will be applied to the simulation of bending fatigue experiments on plain woven glass/epoxy specimens.

4. Simulation of bending fatigue experiments

The fatigue damage model has been implemented in the commercial finite element code SAMCEF™. The integration of the differential equation dD/dN (Equation (22)) for each Gauss-point has been done with the *cycle jump* approach, which has been recently proposed by the authors [66]. Briefly the *cycle jump* approach means that the computation is done for a certain set of loading cycles at deliberately chosen intervals, and that the effect on the stiffness degradation of these loading cycles is extrapolated over the corresponding intervals in an appropriate manner. To this purpose, each Gauss-point has been assigned – beside the damage variable D – a second state variable NJUMP1, which is the number of cycles over which extrapolation is possible without losing reliability and accuracy for that particular Gauss-point. After looping over all Gauss-points, a cumulative relative frequency distribution of the NJUMP1 values is calculated and the overall cycle jump NJUMP (which will be applied to the whole finite element mesh) is determined as a percentile of this frequency distribution.
The local cycle jump NJUMP1 is calculated by imposing a maximum increase in damage ΔD for each particular Gauss-point when the extrapolation would proceed for NJUMP1 cycles. When the increase ΔD is limited to for example 0.01, this is equivalent to a piecewise integration of the damage evolution law for that Gauss-point by dividing the ordinate axis of the damage-cycle history into 100 segments. By decreasing the upper threshold for ΔD for each Gauss-point, the damage evolution law dD/dN will be integrated more accurately, but the global NJUMP – a percentile of the cumulative frequency distribution of all NJUMP1 values – will be smaller and the calculation will proceed more slowly.

The parameters c_i (i=1,…,5) in Equation (22) were determined for the “standard” experiment Pr05_2 which was already shown in Figure 3. Since the fatigue damage model is not at all a

curve-fitting model, the value of the constants c_i (i=1,…,5) were of course retained when simulating other loading conditions. Figure 7 shows the experimental and the simulated force-cycle history for the fatigue test Pr05_2. The imposed displacement varied between zero (stress ratio R = 0 for all Gauss-points) and u_{max} = 30.4 mm and the frequency was 2.2 Hz.

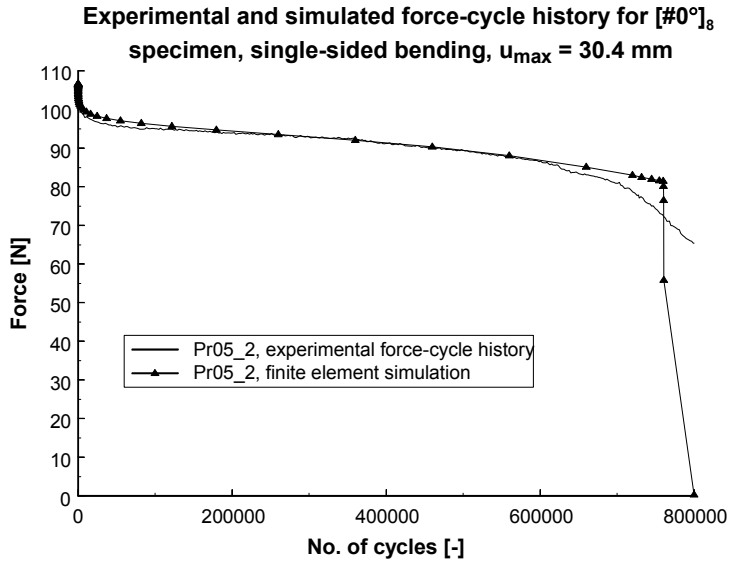

Figure 7 Experimental and simulated force-cycle history.

The parameters were optimized with a non-linear optimization procedure. The final values of all constants in the model are listed in Table 1. The in-plane elastic properties of the $[\#0°]_8$ composite laminates were determined using the dynamic modal analyis method described by Sol et al. [67,68], while the static strength values were determined with an Instron hydraulic testing machine.

Table 1 Material and model constants.

Material parameters		Model parameters	
E_{11} [GPa]	24.57	c_1 [1/cycle]	0.002
E_{22} [GPa]	23.94	c_2 [-]	30.0
ν_{12} [-]	0.153	c_3 [1/cycle]	$4.0 \cdot 10^{-6}$
G_{12} [GPa]	4.83	c_4 [-]	0.85
X_T [MPa]	390.7	c_5 [-]	93.0
X_C [MPa]	345.1		

The determination of the parameters c_i (i=1,…,5) can be split up in two parts in order to reduce the optimization time. Indeed, since the damage initiation function should be able to account for the stage I decrease of the stiffness, the first sharp decline of the force-cycle history can be used to determine the parameters c_1 and c_2. Then the parameters c_3, c_4 and c_5 can be determined for the full force-cycle history.

The effect of the material constants c_1 and c_2 on the behaviour of the damage initiation function has been illustrated by Figure 8. Only the initiation phase of the force-cycle history in Figure 7 has been recalled. The first simulation (c_1 = 0.002; c_2 = 30.0) is the reference simulation. For the second simulation, the value of c_1 has been doubled, resulting in a larger damage initiation. For the third simulation, the value of c_2 has been divided by two. Then the saturation value for damage initiation is increased and the force-cycle history drops down far lower.

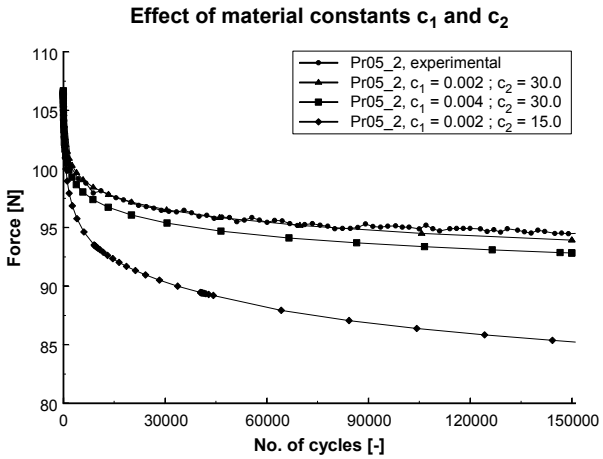

Figure 8 Effect of the material constants c_1 and c_2.

Figure 9 illustrates why the distinction between damage growth under tensile and compressive stresses was necessary. The initiation phase of the force-cycle history in Figure 7 has been recalled again, together with three numerical simulations. For all simulations, the constants c_1 and c_2 have been set to 0.002 and 30.0 respectively, and the power of the damage initiation function for compressive stresses has been set to 3, 2 and 1.

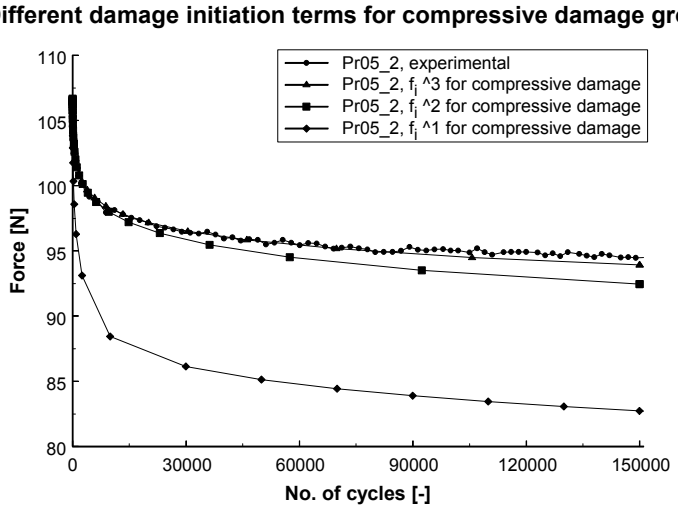

Figure 9 Different equations for damage initiation under compressive loading.

It can be seen that the third power of the damage initiation function provides the best simulation.

Once the material constants c_1 and c_2 have been determined, the constant c_3 can be optimized for the damage propagation phase, which is characterized by a gradual decrease of the stiffness, and hence of the measured bending force.
Figure 10 shows the full experimental and simulated force-cycle history for $c_3 = 4.0 \times 10^{-6}$ and $c_3 = 8.0 \times 10^{-6}$. Clearly, final failure occurs much earlier if the damage propagation rate is increased.

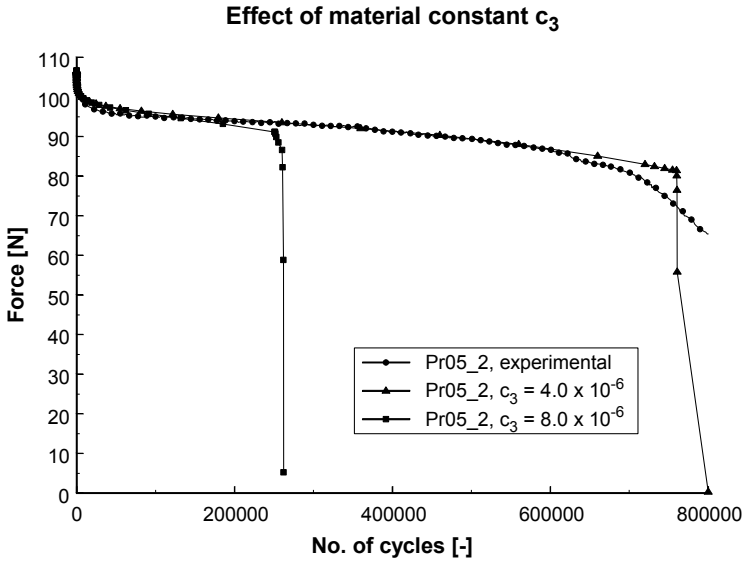

Figure 10 Effect of material constant c_3.

Figure 11 finally shows the damage acceleration factor $1+\exp[c_5(\Sigma-c_4)]$ for $c_4 = 0.85$ and $c_5 = 93.0$. If the fatigue failure index Σ crosses the threshold c_4, the damage acceleration factor forces the damage growth rate to increase explosively.

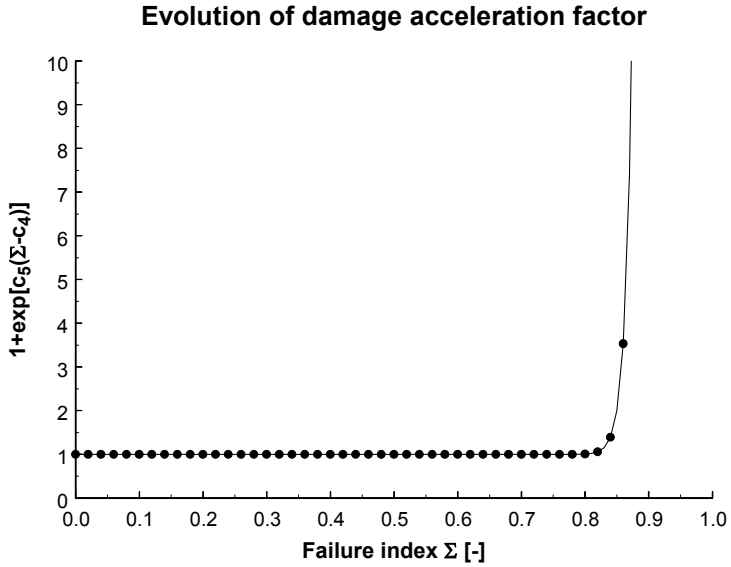

Figure 11 Evolution of the damage acceleration factor accounting for final failure.

Figure 12 shows the calculated stress distribution at the clamped cross-section during fatigue life for the fatigue experiment Pr05_2 which was shown in Figure 7. The abscissa contains the normal stress (tensile stresses are positive, compressive stresses are negative), while the ordinate axis represents the full thickness of the specimen ($y \in$ [-1.36 mm, +1.36 mm]). This numerical simulation shows that the fatigue damage model is capable of simulating redistributing stress states inside the material during fatigue life. Moreover, the stress distribution provides important information about the first locus of failure. Indeed, it was observed from the experimental test Pr05_2 that failure occurred first at the tensile side, and this was confirmed by Figure 12 (stress curve at cycle 660,191).

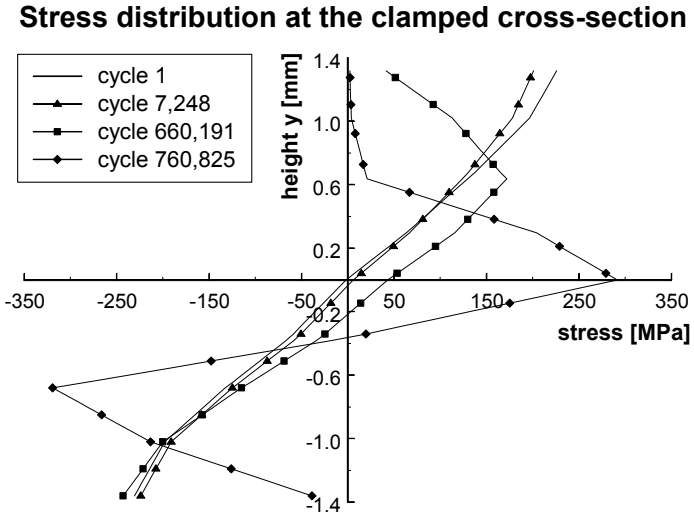

Figure 12 Calculated stress redistribution at the clamped cross-section during fatigue life.

The fatigue damage model is now applied to another experiment Pr10_4 where the imposed displacement u_{max} is much larger: u_{max} = 34.4 mm. The material and model parameters are retained (see Table 1). The experimental and simulated results are shown in Figure 13, together with the experimental and simulated results of the "standard" experiment.

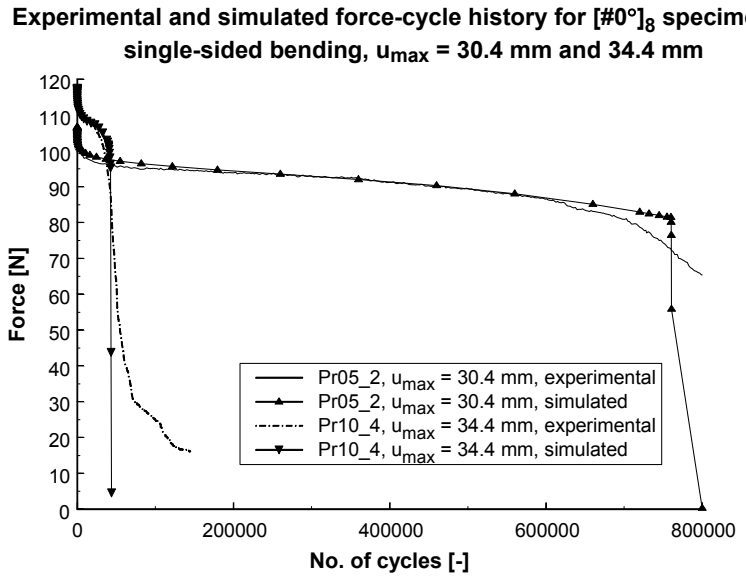

Figure 13 Experimental and simulated force-cycle histories for u_{max} = 30.4 mm and u_{max} = 34.4 mm.

It is clearly shown that the fatigue damage model can predict stiffness degradation and final failure very well, despite the large difference in scale with the "standard" experiment for which the model parameters c_i were determined. Indeed, although failure now occurs almost 700,000 cycles earlier, the fatigue damage model predicts the moment of failure quite accurately. The failure in the experimental test is more gradual though, as can be seen on Figure 14, where the experimental and simulated results for the Pr10_4 experiment are repeated, but with an adjusted scale for the number of cycles (the meaning of the arrows will be explained later).

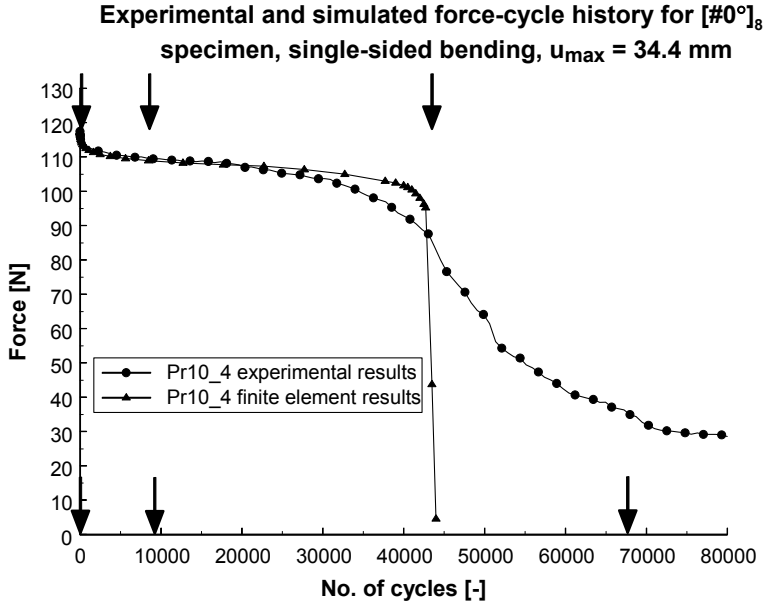

Figure 14 Experimental and simulated force-cycle history of $[\#0°]_8$ specimen for u_{max} = 34.4 mm.

Indeed, the predicted failure is more sudden than the experimentally observed failure, but this is due to the modelling assumptions. Each element of the finite element mesh has the same homogenized elastic and strength properties. If one element at the tensile surface near the clamped cross-section fails, all its neighbours in the width direction of the specimen fail as well. On the other hand, the experimental material is a plain woven glass/epoxy composite, and the experimentally observed failure does not occur at the same time for all material points in the width direction, because the undulating reinforcement pattern causes a more gradual failure.

It is also worth to mention that the recently developed cycle jump approach [66] works very good. At the first few cycles, when there is a sharp decline of the bending force due to matrix cracking, the cycle jumps are very small, but once the stiffness is gradually decreasing in stage II, the cycle jump accelerates. At the end of stage II, the damage growth rate increases again and the cycle jumps are smaller again to accurately evaluate the differential equation for damage growth dD/dN.
Figure 15 shows again the finite element simulation for the Pr10_4 specimen, but now with only the damage initiation function present in the Equation (22) for the damage growth rate dD/dN. It clearly proves that the damage initiation function indeed accounts for the stage I decline of the stiffness, without any contribution of the damage propagation function. The scale of the ordinate axis has been adjusted to clearly show the sharp initial decline of the bending stiffness.

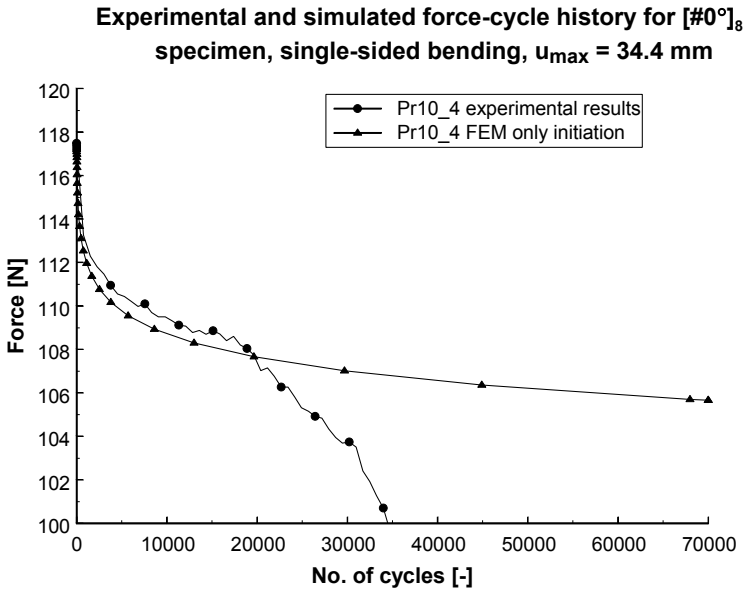

Figure 15 Finite element simulation without the damage propagation function.

A final validation is done by comparing the out-of-plane displacement profile of the experiments and finite element simulations. To that purpose, an improved digital phase-shift shadow Moiré method has been developed by the authors [69]. The proposed method is very efficient and eliminates all causes of erroneous measurements due to miscalibration of phase-stepping devices. By means of this method, the bending profile of the specimen is recorded at regular times during fatigue life. Here, these bending profiles are compared against the

simulated out-of-plane displacements for several cycle numbers which are indicated in Figure 14. The arrows below in Figure 14 indicate the cycle numbers at which a recording of the bending shape was made. The arrows above indicate the cycle numbers at which the simulated bending profile was taken. Of course, due to the discrete cycle jumps, the results of the finite element simulation are only known at discrete loading cycles which are not necessarily the same as the ones at which the bending profile was experimentally recorded. However the evaluation has been done at the best corresponding loading states and the results are shown in Figure 16.

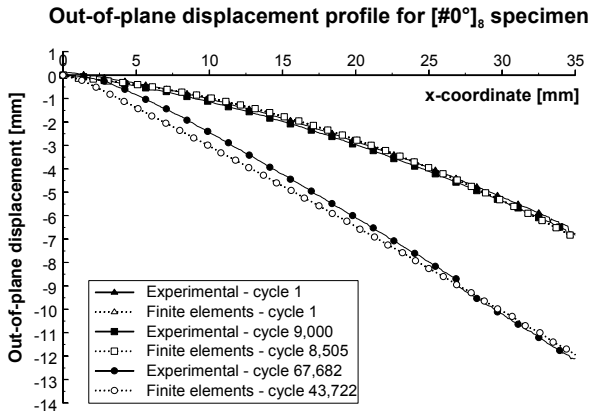

Figure 16 Experimental and simulated out-of-plane displacement profile at several stages in fatigue life.

This Figure clearly shows that at the end of fatigue life, a sort of "hinge" is formed at the clamped cross-section and that the parts remote from the fixation are completely unloaded. It is worthwile to note that although continuum damage mechanics are not suited to model localized phenomena, the introduction of the damage acceleration factor simulates very well the localized fibre fracture at the clamped cross-section. The formation of such a "hinge" leads of course to an enormous increase in strain, which is confirmed by Figure 17 showing the calculated strain distribution during fatigue life at the clamped cross-section.

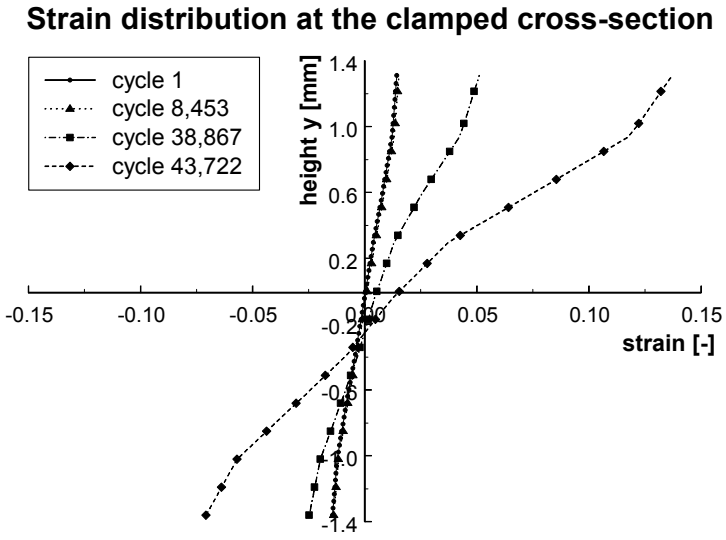

Figure 17 Strain distribution at the clamped cross-section.

This phenomenon again proves the adequacy of the proposed fatigue damage model. Indeed, the damage is very severe at the clamped cross-section and as a consequence, the nominal stress decreases very fast ($\sigma = E_0(1-D)\varepsilon$). But the effective stress $\sigma/(1-D)$, which equals $E_0\varepsilon$, keeps increasing, because the imposed displacement remains the same and due to the severely deteriorated bending stiffness of the clamped cross-section, the strains are increasing very fast.

Conclusions

A new coupled approach of residual stiffness and strength has been proposed for modelling fatigue of fibre-reinforced composites. The fatigue damage model is governed by a scalar damage variable D which is a measure for the degradation of longitudinal stiffness under uni-axial bending. Two new elements have been introduced in the model formulation: (i) the damage growth rate equation has been split up in two terms, separately accounting for damage initiation and propagation, respectively, and (ii) the stress measure has been derived from a modified use of the static Tsai-Wu failure criterion which enables the model to correlate stiffness and strength and to simulate the third stage of final failure, although the model is in fact based on the residual stiffness approach.
The model has been applied to displacement-controlled bending fatigue tests, and it has been shown that the model is capable of simulating the three stages of stiffness degradation: initial decline, gradual reduction and final failure. The force-cycle history and out-of-plane bending profiles have been used for comparison with numerical results.
Although the fatigue model is one-dimensional, and delaminations have not been taken into account, the model in its present form has some attractive features: (i) simulation of whole fatigue life from early stiffness reduction to final failure, (ii) relation with static strength properties through the definition of the fatigue failure index, (iii) limited number of material constants that can be easily determined, and (iv) efficient implementation in commercial finite element code.

Acknowledgements

The author W. Van Paepegem gratefully acknowledges his finance through a grant of the Fund for Scientific Research – Flanders (F.W.O.), and the advice and technical support of the SAMTECH company. The authors also express their gratitude to Syncoglas for their support and technical collaboration.

References

[1] Curtis, P.T. (1989). The fatigue of organic matrix composite materials. In : Partridge, I.K. (ed.). Advanced composites. Londen, Elsevier, pp. 331-367.

[2] Highsmith, A.L. and Reifsnider, K.L. (1982). Stiffness-reduction mechanisms in composite laminates. In : Reifsnider, K.L. (ed.). Damage in composite materials. ASTM STP 775. American Society for Testing and Materials, pp. 103-117.

[3] Masters, J.E. and Reifsnider, K.L. (1982). An investigation of cumulative damage development in quasi-

isotropic graphite/epoxy laminates. In : Reifsnider, K.L. (ed.). Damage in composite materials. ASTM STP 775. American Society for Testing and Materials, pp. 40-62.

[4] Gao, F., Boniface, L., Ogin, S.L., Smith, P.A. and Greaves, R.P. (1999). Damage accumulation in woven-fabric CFRP laminates under tensile loading : Part 1. Observations of damage accumulation. Composites Science and Technology, 59, 123-136.

[5] Fujii, T., Amijima, S. and Okubo, K. (1993). Microscopic fatigue processes in a plain-weave glass-fibre composite. Composites Science and Technology, 49, 327-333.

[6] Degrieck, J. and Van Paepegem, W. (2001). Fatigue Damage Modelling of Fibre-Reinforced Composite Materials: Review. Applied Mechanics Review 54(4), 279-300.

[7] Allen, D.H., Highsmith, A.L. and Lo, D.C. (1990). A continuum damage mechanics model for life prediction of laminated composites. In : Cardon, A.H. and Verchery, G. (eds.). Durability of polymer based composite systems for structural applications. Proceedings of the International Colloquium, 27-31 August 1990, Brussels, Belgium, Elsevier, pp. 119-128.

[8] Shokrieh, M.M. and Lessard, L.B. (2000). Progressive fatigue damage modeling of composite materials, Part I: Modeling. Journal of Composite Materials, 34(13), 1056-1080.

[9] Talreja, R. (2000). Fatigue damage evolution in composites - A new way forward in modeling. In: Proceedings of the Second International Conference on Fatigue of Composites. 4-7 June 2000, Williamsburg, pp. 9.1.

[10] Shokrieh, M.M. and Lessard, L.B. (1997). Multiaxial fatigue behaviour of unidirectional plies based on uniaxial fatigue experiments - I. Modelling. International Journal of Fatigue, 19(3), 201-207.

[11] Shokrieh, M.M. and Lessard, L.B. (1997). Multiaxial fatigue behaviour of unidirectional plies based on uniaxial fatigue experiments - II. Experimental evaluation. International Journal of Fatigue, 19(3), 209-217.

[12] Shokrieh, M.M. and Lessard, L.B. (1998). Residual fatigue life simulation of laminated composites. In : Gowayed, Y. and Abd El Hady, F. (eds.). Proceedings of the International Conference on Advanced Composites (ICAC 98), 15-18 December 1998, Hurghada, Egypt, pp. 79-86
.

[13] Shokrieh, M.M. (1996). Progressive fatigue damage modelling of composite materials. Ph.D. Thesis, McGill University, Montréal, Canada
.

[14] Shokrieh, M.M. and Lessard, L.B. (2000). Progressive fatigue damage modeling of composite materials, Part II: Material characterization and model verification. Journal of Composite Materials, 34(13), 1081-1116
.

[15] Talreja, R. (1986). Stiffness properties of composite laminates with matrix cracking and interior delamination. Engineering Fracture Mechanics, 25(5/6), 751-762.

[16] Talreja, R. (1990). Damage mechanics of composite materials based on thermodynamics with internal variables. In : Cardon, A.H. and Verchery, G. (eds.). Durability of polymer based composite systems for structural applications. Proceedings of the International Colloquium, 27-31 August 1990, Brussels, Belgium, Elsevier, pp. 65-79.

[17] Talreja, R., Yalvac, S., Yats, L.D. and Wetters, D.G. (1992). Transverse cracking and stiffness reduction in cross-ply laminates of different matrix toughness. Journal of Composite Materials, 26(11), 1644-1663.

[18] Sidoroff, F. and Subagio, B. (1987). Fatigue damage modelling of composite materials from bending tests. In : Matthews, F.L., Buskell, N.C.R., Hodgkinson, J.M. and Morton, J. (eds.). Sixth International Conference on Composite Materials (ICCM-VI) & Second European Conference on Composite Materials (ECCM-II) : Volume 4. Proceedings, 20-24 July 1987, London, UK, Elsevier, pp. 4.32-4.39.

[19] Vieillevigne, S., Jeulin, D., Renard, J. and Sicot, N. (1997). Modelling of the fatigue behaviour of a unidirectional glass epoxy composite submitted to fatigue loadings. In : Degallaix, S., Bathias, C. and Fougères, R. (eds.). International Conference on fatigue of composites. Proceedings, 3-5 June 1997, Paris, France, La Société Française de Métallurgie et de Matériaux, pp. 424-430.

[20] Kawai, M. (1999). Damage mechanics model for off-axis fatigue behavior of unidirectional carbon fiber-reinforced composites at room and high temperatures. In: Massard, T. and Vautrin, A. (eds.). Proceedings of the Twelfth International Conference on Composite Materials (ICCM-12). Paris, France, 5-9 July 1999, pp. 322.

[21] Whitworth, H.A. (1998). A stiffness degradation model for composite laminates under fatigue loading. Composite Structures, 40(2), 95-101.

[22] Yang, J.N., Jones, D.L., Yang, S.H. and Meskini, A. (1990). A stiffness degradation model for graphite/epoxy laminates. Journal of Composite Materials, 24, 753-769.

[23] Yang, J.N., Lee, L.J. and Sheu, D.Y. (1992). Modulus reduction and fatigue damage of matrix dominated composite laminates. Composite Structures, 21, 91-100.

[24] Brøndsted, P., Andersen, S.I. and Lilholt, H. (1997). Fatigue damage accumulation and lifetime prediction of GFRP materials under block loading and stochastic loading. In : Andersen, S.I., Brøndsted, P., Lilholt, H., Lystrup, Aa., Rheinländer, J.T., Sørensen, B.F. and Toftegaard, H. (eds.). Polymeric Composites - Expanding the Limits. Proceedings of the 18th Risø International Symposium on Materials Science, 1-5 September 1997, Roskilde, Denmark, Risø International Laboratory, pp. 269-278.

[25] Brondsted, P., Lilholt, H. and Andersen, S.I. (1997). Fatigue damage prediction by measurements of the stiffness degradation in polymer matrix composites. In : Degallaix, S., Bathias, C. and Fougères, R. (eds.). International Conference on fatigue of composites. Proceedings, 3-5 June 1997, Paris, France, La Société Française de Métallurgie et de Matériaux, pp. 370-377.

[26] Hahn, H.T. and Kim, R.Y. (1976). Fatigue behaviour of composite laminates. Journal of Composite Materials, 10, 156-180.

[27] O'Brien, T.K. and Reifsnider, K.L. (1981). Fatigue damage evaluation through stiffness measurements in boron-epoxy laminates. Journal of Composite Materials, 15, 55-70.

[28] Hwang, W. and Han, K.S. (1986). Cumulative damage models and multi-stress fatigue life prediction. Journal of Composite Materials, 20, 125-153.

[29] Schulte, K., Baron, Ch., Neubert, H., Bader, M.G. , Boniface, L., Wevers, M., Verpoest, I. and de Charentenay, F.X. (1985). Damage development in carbon fibre epoxy laminates : cyclic loading. In : Proceedings of the MRS-symposium "Advanced Materials for Transport", November 1985, Strassbourg, 8 p
.

[30] Schulte, K., Reese, E. and Chou, T.-W. (1987). Fatigue behaviour and damage development in woven fabric and hybrid fabric composites. In : Matthews, F.L., Buskell, N.C.R., Hodgkinson, J.M. and Morton, J. (eds.). Sixth International Conference on Composite Materials (ICCM-VI) & Second European Conference on Composite Materials (ECCM-II) : Volume 4. Proceedings, 20-24 July 1987, London, UK, Elsevier, pp. 4.89-4.99
.

[31] Schulte, K. (1984). Stiffness reduction and development of longitudinal cracks during fatigue loading of composite laminates. In : Cardon, A.H. and Verchery, G. (eds.). Mechanical characterisation of load bearing fibre composite laminates. Proceedings of the European Mechanics Colloquium 182, 29-31 August 1984, Brussels, Belgium, Elsevier, pp. 36-54
.

[32] Reifsnider, K.L. (1987). Life prediction analysis : directions and divagations. In : Matthews, F.L., Buskell, N.C.R., Hodgkinson, J.M. and Morton, J. (eds.). Sixth International Conference on Composite Materials (ICCM-VI) & Second European Conference on Composite Materials (ECCM-II) : Volume 4. Proceedings, 20-24 July 1987, London, UK, Elsevier, pp. 4.1-4.31
.

[33] Curtis, P.T. (1989). The fatigue behaviour of fibrous composite materials. Journal of Strain Analysis, 24(4), 235-244
.

[34] Schulte, K. and Masson, J.J. (1989). Damage development in carbon fibre reinforced composite laminates under compressive static and fatigue loading. Developments in the science and technology of composite materials. Proceedings of the Third European Conference on Composite Materials (ECCM/3),

20-23 March 1989, Bordeaux, France, Elsevier Applied Science, pp. 501-507.
.

[35] Gamstedt, E.K. and Sjogren, B.A. (1999). Micromechanisms in tension-compression fatigue of composite laminates containing transverse plies. Composites Science and Technology, 59(2), 167-178.

[36] Kachanov, L.M. (1958). On creep rupture time. Izv. Acad. Nauk SSSR, Otd. Techn. Nauk, No.8, 26-31.

[37] Kachanov, L.M. (1986). Introduction to continuum damage mechanics. Dordrecht, Martinus Nijhoff Publishers, 135 pp.

[38] Rabotnov, Yu.N. (1969). Creep rupture - Proceedings of the XII International Conference on Applied Mechanics. Stanford, Springer Berlin.

[39] Lemaitre, J. (1971). Evaluation of dissipation and damage in metals, submitted to dynamic loading. Proceedings I.C.M. I, Kyoto, Japan.

[40] Krajcinovic, D. and Lemaitre, J. (eds.) (1987). Continuum damage mechanics: theory and applications. Wien, Springer - Verlag, 294 pp.

[41] Chaboche, J.L. (1988). Continuum damage mechanics : part I - General concepts. Journal of Applied Mechanics, 55, 59-64.

[42] Chaboche, J.L. (1988). Continuum damage mechanics : part II - Damage growth, crack initiation and crack growth. Journal of Applied Mechanics, 55, 65-72.

[43] Krajcinovic, D. (1985). Continuous damage mechanics revisited : basic concepts and definitions. Journal of Applied Mechanics, 52, 829-834.

[44] Sidoroff, F. (1984). Damage mechanics and its application to composite materials. In : Cardon, A.H. and Verchery, G. (eds.). Mechanical characterisation of load bearing fibre composite laminates. Proceedings of the European Mechanics Colloquium 182, 29-31 August 1984, Brussels, Belgium, Elsevier, pp. 21-35.

[45] Reifsnider, K.L. (1986). The critical element model : a modeling philosophy. Engineering Fracture Mechanics, 25(5/6), 739-749.

[46] Leus, G. (1999). Damage models for the impact behaviour of composites. Doctoral thesis (in Dutch). Universiteit Gent, Belgium, 251 pp.

[47] Verleysen, Patricia (1999). Experimental study and numerical modelling of the dynamic behaviour in tension of a fibre-reinforced quasi-brittle material. Doctoral thesis (in Dutch). Universiteit Gent, Belgium, 302 pp.

[48] Ogin, S.L., Smith, P.A. and Beaumont, P.W.R. (1985). Matrix cracking and stiffness reduction during the fatigue of a (0/90)s GFRP laminate. Composites Science and Technology, 22(1), 23-31.

[49] Beaumont, P.W.R. (1990). The mechanics of fatigue damage in structural composite materials. In : Füller, J., Grüninger, G., Schulte, K., Bunsell, A.R. and Massiah, A. (eds.). Developments in the science and technology of composite materials. Proceedings of the Fourth European Conference on Composite Materials (ECCM/4), 25-28 September 1990, Stuttgart, Elsevier Applied Science, pp. 195-205.

[50] Beaumont, P.W.R. (1987). The fatigue damage mechanics of composite laminates. In : Wang, A.S.D. and Haritos, G.K. (eds.). Damage mechanics in composites. Presented at the Winter Annual Meeting of the ASME, 13-18 December 1987, Boston, Massachusetts, ASME, pp. 53-63.

[51] Salkind, M.J. (1972). Fatigue of composites. In: Corten, H.T. (ed.). Composite Materials Testing and Design (Second Conference). ASTM STP 497. Baltimore, American Society for Testing and Materials, pp. 143-169.

[52] Tsai, S.W. and Wu, E.M. (1971). A general theory of strength for anisotropic materials. Journal of Composite Materials, 5, 58-80.

[53] Wu, E.M. (1972). Optimal experimental measurements of anisotropic failure tensors. Journal of Composite Materials, 6, 472-489.

[54] Liu, K.-S. and Tsai, S.W. (1998). A progressive quadratic failure criterion for a laminate. Composites Science and Technology, 58, 1023-1032.

[55] Halpin, J.C., Jerina, K.L. and Johnson, T.A. (1973). Characterization of composites for the purpose of reliability evaluation. In: Analysis of the test methods for high modulus fibers and composites. ASTM STP 521, pp. 5-64.

[56] Yang, J.N. and Jones, D.L. (1981). Load sequence effects on the fatigue of unnotched composite materials. In : Lauraitis, K.N. (ed.). Fatigue of fibrous composite materials. ASTM STP 723. Philadelphia, American Society for Testing and Materials, pp. 213-232.

[57] Schaff, J.R. and Davidson, B.D. (1997). Life prediction methodology for composite structures. Part I - Constant amplitude and two-stress level fatigue. Journal of Composite Materials, 31(2), 128-157.

[58] Schaff, J.R. and Davidson, B.D. (1997). Life prediction methodology for composite structures. Part II - Spectrum fatigue. Journal of Composite Materials, 31(2), 158-181.

[59] Caprino, G. and D'Amore, A. (1998). Flexural fatigue behaviour of random continuous-fibre-reinforced thermoplastic composites. Composites Science and Technology, 58, 957-965.

[60] Lee, C.-H. and Jen, M.-H.R. (2000). Fatigue response and modelling of variable stress amplitude and frequency in AS-4/PEEK composite laminates. Part 1: Experiments. Journal of Composite Materials, 34(11), 906-929.

[61] Lee, C.-H. and Jen, M.-H.R. (2000). Fatigue response and modelling of variable stress amplitude and frequency in AS-4/PEEK composite laminates. Part 2: Analysis and formulation. Journal of Composite Materials, 34(11), 930-953.

[62] Hibbeler, R.C. (1997). Mechanics of Materials. Third Edition. New Jersey, Prentice-Hall Inc., pp. 87-90.

[63] Boniface, L., Ogin, S.L. and Smith, P.A. (1993). Damage development in woven glass fibre/epoxy laminates under tensile loading. In : Materials science division of the Institute of Materials (ed.). Second International Conference on deformation and fracture of composites. Proceedings, 29-31 March 1993, Manchester, UK, the Institute of Materials, pp. 33.1-33.10.

[64] Van Paepegem, W. and Degrieck, J. (2001). Experimental setup for and numerical modelling of bending fatigue experiments on plain woven glass/epoxy composites. Composite Structures, 51(1), 1-8.

[65] Van Paepegem, W. and Degrieck, J. (2000). Numerical modelling of fatigue degradation of fibre-reinforced composite materials. In: Topping, B.H.V. (ed.). Proceedings of the Fifth International Conference on Computational Structures Technology. Volume F: Computational Techniques for Materials, Composites and Composite Structures, Leuven, 6-8 September 2000, Civil-Comp Press, pp. 319-326.

[66] Van Paepegem, W., Degrieck, J. and De Baets, P. (2001). Finite Element Approach for Modelling Fatigue Damage in Fibre-reinforced Composite Materials. Composites Part B, 32(7), 575-588.

[67] Sol, H. and de Wilde, W.P. (1988). Identification of elastic properties of composite materials using resonant frequencies. In : Brebbia, C.A., de Wilde, W.P. and Blain, W.R. (eds.). Proceedings of the International Conference "Computer Aided Design in Composite Material Technology", Southampton, 1988, Springer-Verlag, pp. 273-280.

[68] Sol, H. (1990). Identification of the complex moduli of composite materials by a mixed numerical/experimental method. In : de Wilde, W.P. and Blain, W.R. (eds.). Proceedings of the second International Conference on Computer Aided Design in Composite Material Technology, Brussels, 25-27 April 1990, Springer-Verlag, pp. 267-279.

[69] Degrieck, J., Van Paepegem, W. and Boone, P. (2001). Application of digital phase-shift shadow Moiré to micro deformation measurements of curved surfaces. Optics and Lasers in Engineering, 36, 29-40.